Available online at www.sciencedirect.com
SCIENCE DIRECT
Journal of Power Sources 156 (2006) 224–231
JOURNAL OF POWER SOURCES
www.elsevier.com/locate/jpowsour

Effects of sputtering parameters on the performance of electrodes fabricated for proton exchange membrane fuel cells

Kuo-Lin Huang [a,*], Yi-Chieh Lai [b], Cheng-Hsien Tsai [c]

[a] *Department of Environmental Engineering and Science, National Pingtung University of Science and Technology, 1 Hseuh Fu Road, Neipu, Pingtung 91201, Taiwan*
[b] *Department of Environmental Engineering, National Cheng Kung University, Tainan 70101, Taiwan*
[c] *Department of Chemical and Material Engineering, National Kaohsiung University of Applied Sciences, Kaohsiung 807, Taiwan*

Received 19 April 2005; received in revised form 24 May 2005; accepted 27 May 2005
Available online 22 July 2005

Abstract

One way to alleviate the emission of air pollutants and CO_2 due to burning fossil fuels is the use of fuel cells. Sputter deposition techniques are good candidates for the fabrication of electrodes used for proton exchange membrane fuel cells (PEMFCs). Input power and sputtering-gas pressure are two important parameters in a sputtering process. However, little is known about the effects of these sputtering parameters on the performance of PEMFC electrodes. Therefore, this study applied a radio frequency (RF) magnetron sputter deposition process to prepare PEMFC electrodes and investigated the effects of RF power and sputtering-gas pressure in electrode fabrication on electrode/cell performance. At a Pt loading of 0.1 mg cm^{-2}, the electrode fabricated at 100 W, 10^{-3} Torr was found to exhibit the best performance mainly due to its lowest kinetic (activation) resistance (dominating the cell performance) in comparison to those fabricated by 50 and 150 W at 10^{-3} Torr, as well as by 10^{-4} and 10^{-2} Torr at 100 W. In the tested ranges, the control of sputtering-gas pressure seems to be more critical than that of RF power for the activation loss. In addition to electrochemically active surface area, electrode microstructure should also be responsible for electrode/cell polarization, particularly the activation polarization.

Keywords: Proton exchange membrane fuel cells; RF sputtering; Pt deposition; Electrode fabrication

1. Introduction

The use of fuel cells may alleviate the emission of air pollutants and CO_2 resulted from utilizing fossil fuels [1]. Presently, the greatest research interest throughout the world has focused on PEMFCs and solid oxide cell stacks [2]; furthermore, the PEMFCs have reached the stage of being in the forefront among the different types of fuel cells [3]. The most studied fuels for the PEMFCs are hydrogen and methanol; however, the former, without any methanol crossover concern, has a higher power density output than the latter [4,5]. A single H_2–O_2/air PEMFC is chiefly comprised of three types of components: a membrane-electrode assembly (MEA), two bipolar plates (having flow fields or separators), and two seals; in its simplest form, the MEA consists of a membrane, two dispersed catalyst layers, and two gas diffusion layers (GDL) [6].

The MEA is the heart of a PEMFC [3] and there are two modes of MEA fabrication: (I) application of the catalyst layer to the GDL followed by membrane addition or (II) application of the catalyst layer to the membrane followed by GDL addition [6]. MEAs rely on different catalyst preparation methods such as impregnation reduction, spreading, spraying, catalyst powder deposition, catalyst decaling, painting, electro-deposition, and sputter deposition in combination with hot-pressing procedures to bond disparate carbon

* Corresponding author. Tel.: +886 8 770 3202x7092; fax: +886 8 774 0256.
E-mail address: huangkL@mail.npust.edu.tw (K.-L. Huang).

0378-7753/$ – see front matter © 2005 Elsevier B.V. All rights reserved.
doi:10.1016/j.jpowsour.2005.05.088

cloth electrodes to an electrolytic membrane [6–10]. (The last two methods mentioned belong to the Modes I or II whereas the others are the Mode I for MEA fabrication.) Improved processes use thinner active layer thickness (i.e., from 100 to 25 μm) and smaller carbon-supported nanometer size Pt particles (<10 nm, i.e., 2.5 nm average for E-TEK) to enhance the Pt utilization and reduce the Pt amount in gas diffusion electrodes (GDEs) [9,11]. Therefore, the Pt loading in the conventional GDEs has been lowered from early 4 to recent 0.4 mg cm^{-2} [8,12], very crucial for H_2–O_2/air PEMFCs to be commercially realizable [6,8,9,13,14].

Among the electrode fabrication methods aforementioned, electro-deposition [13–16] and sputter deposition [8,12,17] techniques can be used to localize Pt within the (membrane carbon interface) regions responsible for electrochemical reaction in MEAs; the purpose of this design is to increase the electrode Pt utilization by diminishing inactive catalyst sites when compared to most of the other methods with Pt more uniformly dispersed in the whole GDE. The plasma sputter deposition technique has a high potential for MEA fabrication to reduce cell costs by achieving ultra-low levels of Pt catalyst loading [8]. For example (Mode I type mentioned above for MEA fabrication), it has been found that the oxygen electrode with an ultra-low Pt loading (0.1 mg cm^{-2}) electrocatalyst layer (1 μm thick) sputter-deposited on uncatalyzed GDE exhibits comparable performance to that of a standard E-TEK electrode [17]; additionally, the sputtering of a 50 nm Pt film (0.05 mg cm^{-2}) on the front surface of a fuel cell electrode may diminish overpotentials to improve the electrode/cell performance [11,18]. Recently, using the Mode II methods for MEA fabrication, researchers have found that the electrode fabricated by plasma-sputtering Pt (0.043 mg cm^{-2}) directly on the surface of Nafion electrolyte displays ten times higher efficiency than those prepared by conventional methods [12]; moreover, the performance of a sputter-deposited Nafion membrane with a Pt loading level of 0.04 mg cm^{-2} is comparable to a commercial MEA with a Pt loading of 0.4 mg cm^{-2} [8]. This work did not specifically focus on the electrode Pt localization and loading. Instead, we are concerned about the electrode/cell performance (mainly regulated by the gas/proton/electron (triple access) continuity) achieved at various sputtering conditions [8,12].

However, little is known about the effects of RF power and sputtering-gas pressure on the performance of MEAs/electrodes fabricated by sputtering processes. Both RF power and sputtering-gas pressure influence the deposition rates on substrates and the microstructures (microcrystallizationon) of films sputtered because the plasma density and electron kinetic energy vary with the sputter conditions [19–23]. The microstructures of electrode catalysts prepared by sputtering for fuel cells may affect the electrode/cell performance. In this study, therefore, an RF magnetron sputter process was used to sputter Pt in GDEs to prepare the electrodes in MEAs (Mode I type) and they were tested using cell polarization, cyclic voltammetry, ac impedance, and surface analysis techniques to explore how the experimental parameters including RF power and sputtering-gas pressure employed in electrode fabrication influenced the performances of electrodes/MEAs.

2. Experimental

2.1. Preparation of electrodes and MEAs

An RF sputtering system was employed to deposit Pt catalyst onto the carbon particles (ranging ~30–90 nm with an average size of 56 nm; also see Section 3.2) supported by carbon cloth (uncatalyzed Gore gas diffusion electrodes (CARBEL CL, thickness = 0.4 mm), Gore, USA) with a projected active area of 5 cm^2. The base vacuum pressure was set at 4×10^{-5} Torr in each sputtering operation. The Argon flow rates of 15, 30, and 65 sccm were employed to achieve the pressures of 10^{-4}, 10^{-3}, and 10^{-2} Torr, respectively. Three input RF powers (50, 100, and 150 W) were tested.

A α-step surface profiler (Alpha-Step, Tencor 200) was used to measure the thickness of Pt films sputtered onto a planar Si substrate and the Pt loading of a substrate (Pt amount on Pt film projected area in mg cm^{-2}) was calculated by Pt film thickness × Pt density. The measured Pt film thickness divided by sputtering time gave Pt deposition rate (in nm min^{-1}). For convenience, we controlled sputtering time to achieve different Pt loadings on substrates at various operational conditions. By this way, the loadings of Pt sputtered onto uncatalyzed Gore gas diffusion electrodes were estimated. For each test, the anode and cathode Pt loadings were 0.4 and 0.1 mg cm^{-2}, respectively. The polymer membrane electrolyte was Nafion 117 (Dupont, USA). Prior to use, each membrane was first boiled in 3% hydrogen peroxide, then washed with de-ionized water, and finally boiled in 1 M sulfuric acid [8]. The catalyzed anode and cathode and the pretreated membrane were hot-pressed at 120 °C and 5000 lb for 1 min to form the MEA. Fig. 1 schematically depicts the structures of the MEA (the Nafion membrane sandwiched/hot-pressed with the anode and cathode) and catalyzed electrode (with Pt sputtered onto carbon particles supported by carbon cloth) (also see Section 3.2).

2.2. Cell polarization measurements and electrochemical analysis

Screws and nuts were used to assemble a cell with the prepared MEA symmetrically sandwiched by two Teflon gaskets, two carbon (graphite) blocks with gas flow channels, and two copper current collectors. The single cell was then installed on a standard fuel cell test station. After the activation of each MEA in cell, the cell polarization was conducted at 65 °C (80 and 70 °C for the anode and cathode humidifiers, respectively) using the test station. The airflow rates were controlled at 1.5 and 2 times of the stochiometric require-

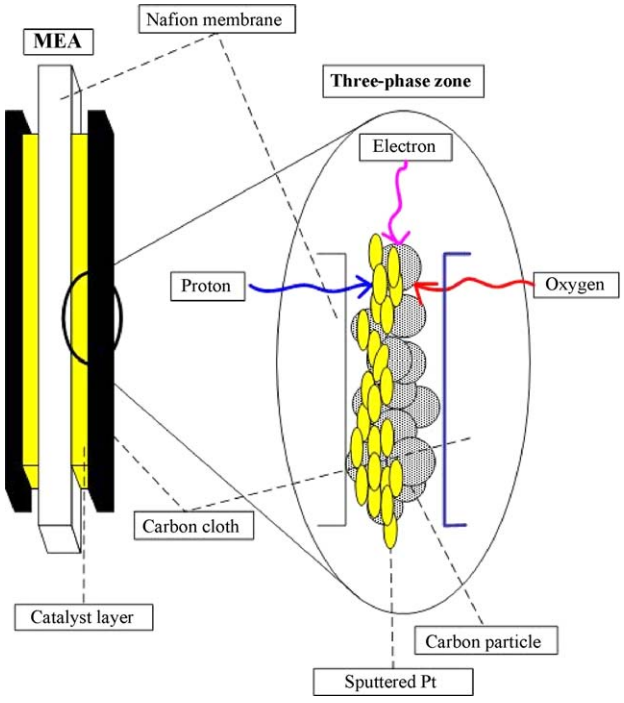

Fig. 1. Schematic representation of the MEA and electrode structures.

ments for the anode and cathode feeding gases (hydrogen and oxygen, respectively).

A potentiostat (CHI 614A Electrochemical Analyzer) + PC system connected with the test station was used to perform cyclic voltammetric (CV) measurements with nitrogen gas passing through the cathode (working electrode) and hydrogen gas through the anode (counter electrode) at a scan rate of 20 mV s^{-1} with the potential cycled between 0 and 1.4 V. The coulombic charge for hydrogen adsorption/desorption obtained in CV was used to calculate the electrochemically active surface (EAS) area of Pt sputtered by assuming that the charge of mono-layer hydrogen adsorption on bright Pt surface was 210 μC cm^{-2} [24]. The same potentiostat system was applied to carry out ac impedance measurements for oxygen reduction reactions in the frequency range of 10 kHz to 0.1 Hz (10 mV amplitude) at 0.7 and 0.8 V using the oxygen cathode (working electrode) and hydrogen anode (counter electrode). Scanning electron microscopy (SEM) (JEOL, JSM-6700F) was used to examine the morphology of Pt layers sputtered.

3. Results and discussion

3.1. Deposition rate of Pt

The Pt sputter deposition rate is mainly affected by the RF power and sputtering-gas pressure of a sputter system. At 10^{-3} Torr, the Pt sputter deposition rate increased with increasing RF power. For the operation of RF powers of 50, 100, and 150 W, the average Pt sputter deposition rates were 22, 39, and 50 nm min^{-1} (corresponding to 0.047, 0.084, and 0.107 mg cm^{-2} min^{-1}, respectively), (Table 1). Similarly, Kawamura et al. [25] found that the Pt deposition rate on a glass substrate increased from 25 to 41 nm min^{-1} when increasing RF powers from 25 to 40 W. This is because the plasma density increased with elevated RF power to generate more Ar^+ resulting in the more Pt bombarded and the elevation of deposition rate [26]. The Pt deposition rates converted to Pt loading rates were in the range of 0.047–0.107 mg cm^{-2} min^{-1}, greater than that (0.039 mg cm^{-2} min^{-1}) in a work performed at 2×10^{-2} Torr, 470 V acceleration voltage/500 mA plate-current [17].

Table 1
Average Pt sputter deposition rates at various RF powers and sputtering-gas pressures

Power (W)	Pressure (Torr)	Pt deposition rate (nm min^{-1})[a]	Pt deposition rate (mg cm^{-2} min^{-1})
50	10^{-3}	22	0.047
100	10^{-3}	39	0.084
150	10^{-3}	50	0.107
100	10^{-2}	33	0.070
100	10^{-4}	28	0.060

[a] The Pt sputter deposition rate was calculated from dividing average Pt film thickness by sputter time (on Si substrates (5 cm^2) in triplicate measurements with a standard deviation below 2 nm min^{-1} for each operation). The base pressure of vacuum system was fixed at 4×10^{-5} Torr during each operation.

In addition, the average Pt deposition rate increased from 33 to 39 nm min^{-1} (0.070–0.084 mg cm^{-2} min^{-1}) when the pressure decreased from 10^{-2} to 10^{-3} Torr while this rate reduced to 28 nm min^{-1} (0.060 mg cm^{-2} min^{-1}) at the operation of 10^{-4} Torr. This is because there is a trade-off between the Ar^+ and its kinetic energy for changing the pressure. Declining pressure may increase the electron mean energy to increase the Pt sputter yield, but decrease the Ar number to reduce the probabilities of Pt atom bombarded away from the target [26,27]. Li et al. [19] also stated a similar trend for the deposition of silicon nitrides from an amorphous silicon disk target onto a Si wafer substrate using an RF system. Their finding is that the deposition rate at 200 W increases as the pressure is reduced from 1.35 to 0.25 Pa but decreases as the pressure is reduced further.

3.2. Effect of RF power applied in electrode fabrication on MEA/cell performances

To evaluate the effect of RF power on the cathode performances of MEAs, the RF power was fixed at 100 W and 10^{-3} Torr for the preparation of Pt/C anodes while 50, 100, and 150 W powers were used to fabricate the cathodes at the same pressure. At the same Pt loading (0.1 mg cm^{-2}), the performance of MEAs with the Pt/C cathode prepared at 50 and 150 W were similar but lower than that prepared at 100 W (Fig. 2). This tendency can be seen also when the cell potential reach 0.8 V, particularly at <0.7 V (with relatively

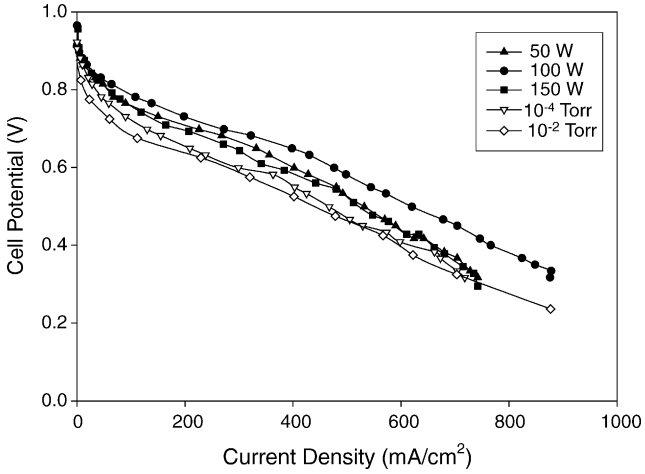

Fig. 2. Current–potential curves for the MEAs with cathodes prepared at different RF powers (under the same sputtering-gas pressure of 10^{-3} Torr) and different sputtering-gas pressures (under the same RF power of 100 W).

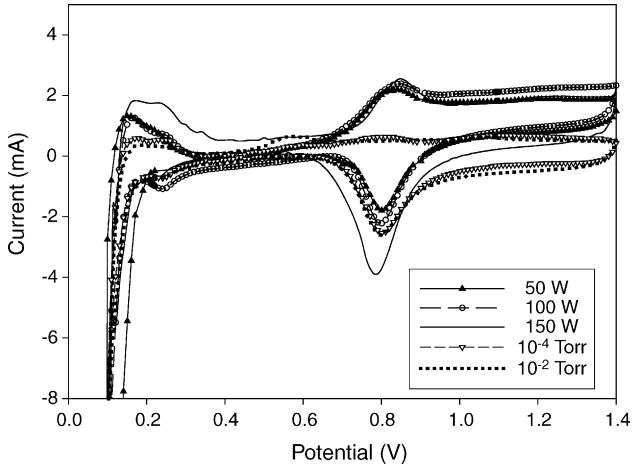

Fig. 3. Cyclic voltammograms for the electrodes prepared at different RF powers and sputtering-gas pressures.

higher overpotentials for oxygen reduction) to obtain middle to high current densities in operation. In cyclic voltammograms, however, the coulombic charge for hydrogen desorption of 100 W case was similar to that of the 50 W case, but apparently smaller than that of 150 W case (Fig. 3). The result leads to the fact that the EAS area of the 100 W case was slightly and evidently smaller than those of the 50 and 150 W cases, respectively (Table 2), and consistent with that the larger Pt grains (on carbon) found for the 100 case than for the other two cases (Fig. 4a and c). Also, the carbon particle matrix was much more porous to enlarge the EAS area for the 150 W case than for the 50 and 100 W cases reflected by their corresponding currents in the non-faradic double layer charging region at 0.4–0.6 V. The sizes of uncatalyzed carbon particles (supported by carbon cloth) on a piece of GDL were approximately 30–90 nm (30–40 nm, 29%; 40–50 nm, 13%; 50–60 nm, 16%; 60–70 nm, 28%; 70–90 nm, 14%) (Fig. 4d) with an average size (d) of 56 nm ($d = (\Sigma\% \times \text{particle size})/100$) [18] based on 100 particles randomly chosen from the SEM photo. After sputtering, although most of the Pt-covered carbon particles displayed size increments in a level of nanometer, the sputtered Pt apparently decreased gas access. For the GDE, Fig. 4e shows that the apparent thickness of carbon particle layer is about 10 μm and the carbon cloth region has fibers obviously observed; via the mapping of Pt, approximately, the sputtered Pt densely locates in the front of the carbon particle layer and some Pt grains widely disperse in the region (mainly the carbon cloth) left to the narrow catalyzed layer (Fig. 4f) verifying the localization of electrode Pt by this sputtering technique.

Nevertheless, all the three electrodes prepared at three corresponding power conditions displayed smaller semicircular loops at 0.8 V than at 0.7 V (Fig. 5a and b, respectively) indicating the electrodes' higher activation resistances at 0.8 V than at 0.7 V in ac impedance measurements [28], consistent with their performance tendency aforementioned. This result is mainly because the electrodes were under the control of charge transfer reaction in the low current density range and the charge transfer resistance decreased as the electrode overpotential increased [29]. However, at both 0.8 and 0.7 V, the electrode prepared at 100 W had a smaller semicircular loop than the other two cases revealing that the charge transfer resistance of oxygen reduction was lower for the electrode prepared at 100 W than for those prepared at 50 and 150 W.

Table 2
Electrode kinetic parameters of oxygen reduction for the MEAs with cathodes (5 cm^2) fabricated at various RF powers and sputtering-gas pressures

Test condition	MEA no.	EAS area ($m^2\ g^{-1}$)	R_p (Ω)	R (Ω)	E_o (V)	I_o (μA cm^{-2})	b (V dec^{-1})
Power (W)							
50	1	6.39	0.63	0.45	0.961	4.62	0.115
100	2	5.30	0.41	0.43	0.965	4.01	0.111
150	3	8.76	0.61	0.48	0.956	4.16	0.115
Pressure (Torr)							
10^{-4}	4	3.11	0.87	0.46	0.962	6.75	0.124
10^{-3}	2	5.30	0.41	0.43	0.965	4.01	0.111
10^{-2}	5	3.40	0.88	0.46	0.927	4.03	0.127

The sputtering-gas pressures were fixed at 10^{-3} Torr for the RF power test while the RF powers were fixed at 100 W for the sputtering-gas pressure test. The Pt loadings for the above five cases were controlled to be very similar (0.1 mg cm^{-2}) in the experiments for the comparison of MEAs prepared at various RF powers and sputtering-gas pressures.

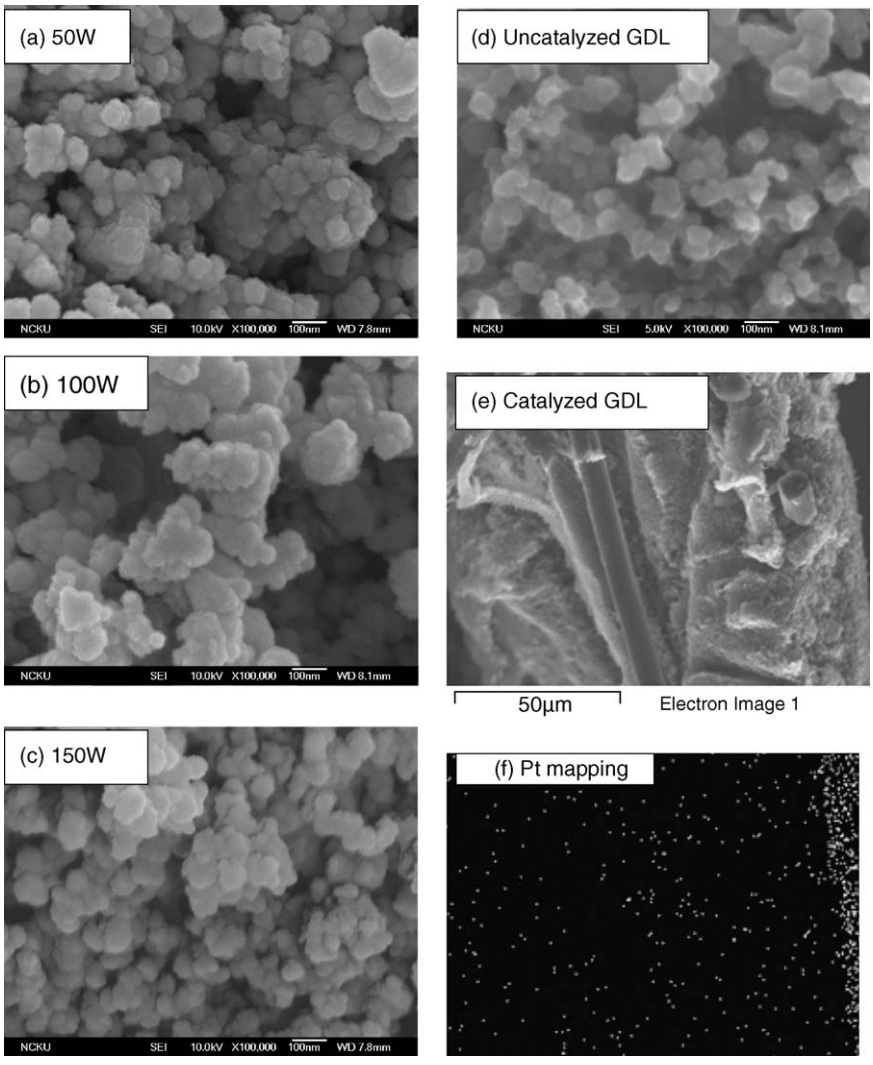

Fig. 4. SEM photos for the electrodes (Pt sputtered onto carbon particles) with a Pt loading of 0.1 mg cm^{-2} fabricated at: (a) 50 W, (b) 100 W, and (c) 150 W (10^{-3} Torr); SEM photos for (d) the uncatalyzed GDE (carbon particles supported by carbon cloth) and (e) the catalyzed GDE (side-view), and (f) Pt mapping (light spots) of the catalyzed GDE.

To analyze the impedance data in more detail, each Nyquist plot obtained at 0.8 V was fitted by a non-linear regression with an equivalent electrical circuit $R(R_pC_{dl})$ (in Fig. 5b), where R was the ohmic resistance (sum of electrode and electrolyte resistance), R_p was the polarization resistance (sum of charge transfer and diffusion resistance), and C_{dl} was the double layer capacity [28,29]. As shown in Table 2, the R-value for the 100 W case was similar to those for the 50 and 150 W cases while the R_p value for the former case was apparently smaller than those for the latter two cases, suggesting the lower polarization resistance (particularly the charge transfer resistance) for the 100 W case than for the 50 and 150 W cases. This finding also supports the trend observed in electrode/MEA performance for the three cases. To gain more kinetic information associated with the cell performance, the electrode kinetic parameters were analyzed from the fitting of cell potential versus current density data using the following two equations [11,28–30]:

$$E = E_o - b \log I - RI \quad (1)$$

$$E_o = E_r + b \log I_o \quad (2)$$

where E, E_o and E_r are the cell potential, open circuit potential and reversible potential, respectively, I_o the exchange current density for oxygen reduction, b the Tafel slope, and R as stated in the data fitting of Nyquist plots, the cell ohmic resistance. Note that each R-value fitted from ac impedance data was plugged into the polarization data fitting to obtain its corresponding b-value in Eq. (1); moreover, due to the apparent slope change of cell polarization curves, the data with cell potentials below 0.6 V were excluded in the curve fitting. The three electrodes fabricated at different RF powers exhibited similar exchange current densities ($\sim 4 \times 10^{-6}$ A cm^{-2}). The same is true for their Tafel slopes, close to 0.12 V dec^{-1}

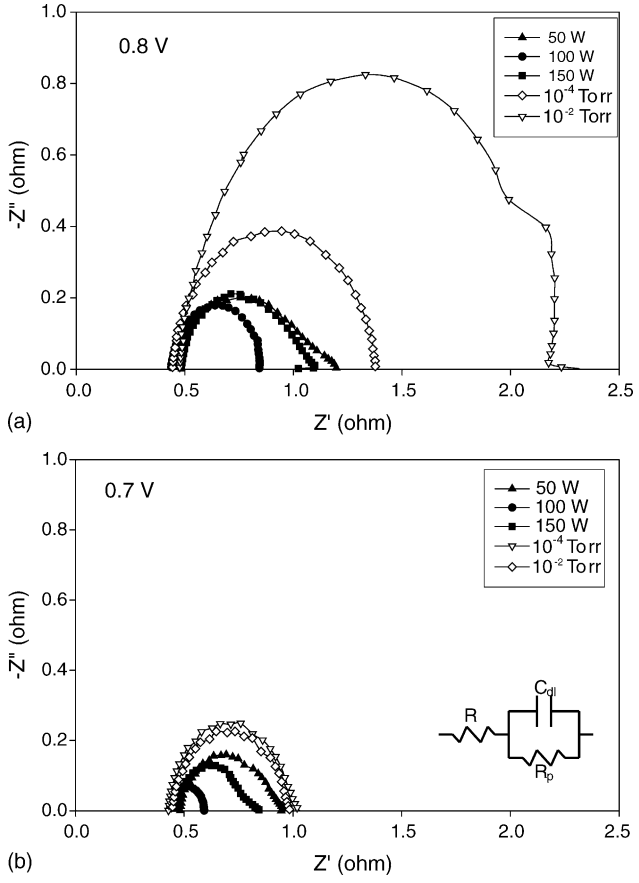

Fig. 5. The ac impedance Nyquist plots at: (a) 0.8 V and (b) 0.7 V (10 kHz to 0.1 Hz) for the electrodes prepared at different RF powers and sputtering-gas pressures.

corresponding to typical oxygen reduction on oxide-free Pt in acid media [31]. In comparison to the 50 and 150 W cases, the 100 W case had a slightly greater E_o to reflect a better kinetic activity, consistent with the R_p trend of these cases determined in ac impedance measurements and partially responsible for its higher MEA performance. This is possible that at the same Pt loading (0.1 mg cm^{-2}), the 100 W case had a better electrode structure (Pt/C configuration) than the other two cases to display a lower polarization resistance.

As mentioned before, the energy of Pt atoms bombarded away from target increased as the RF power increased, which might enhance the adsorption of Pt atoms onto carbon particles to lower the ohmic resistance but some of the Pt atoms might enter the inner micropores of carbon particles or the channels among carbon particles near carbon cloth to lose contact with the bulk Pt film or Nafion electrolyte and thus resulted in a smaller EAS area. When the RF power increased from 50 to 100 W generating larger Pt grains (on carbon) also might lower the EAS area. However, when the plasma power was raised to 150 W, more defects [20] in the crystal growth of Pt grains/film might be present to induce additional electronic ohmic resistance. Similar results were observed for the sizes of Ni grains sputtered onto an Al_2O_3 substrate [20] and those of ZnO grain on a Si substrate largely growing with increasing RF power [21]. (The latter case is mainly because the excessive RF power induces a faster reaction rate and severer surface damage resulting in a poorer crystalline quality of ZnO film and the change of film structure from columnar to plate-like grains when increasing the powers from 150 to 300 W [21].) In this study, the crowded Pt/C particles might also reduce the gas diffusion access to increase the mass transfer resistance of oxygen gas, particularly when the current densities were above 400 mA cm^{-2} (with the polarization mainly due to mass transfer loss). In addition to the real surface electrode area (or EAS area), the surface concentrations of the species involved in the electrode reactions also affect the effective charge transfer resistance [12]. Therefore, the inconsistency between the EAS area and electrode/cell performance indicates that surface concentrations of species (particularly the oxygen) was more responsible than the EAS area for the charge transfer resistance and thus the variation of electrode/cell performance. The electrode microstructure formed at different RF powers should be associated with both the EAS area and the surface concentrations of species involved in the electrode reactions.

3.3. Effect of sputtering-gas pressure in electrode fabrication on MEA/cell performances

In addition to the 10^{-3} Torr, the pressures of 10^{-2} and 10^{-4} Torr were also employed to compare the effects of sputtering-gas pressure in electrode fabrication on the performances of electrodes. With the same electrode Pt loading (0.1 mg cm^{-2}) at 100 W, however, the electrodes made at both the 10^{-2} and 10^{-4} Torr show poorer performances than that made at the 10^{-3} Torr and even than those made at 10^{-3} Torr with different RF powers (50 and 150 W) (Fig. 2).

The I_o values of 10^{-2} and 10^{-3} Torr cases were similar but slightly lower than that of 10^{-4} Torr case, whereas the b-values of these three cases were all close to 0.12 V dec^{-1} (Table 2). Again, the E_o value of 10^{-3} Torr case was slightly higher than that of 10^{-4} Torr case and apparently than that of the 10^{-2} Torr case to be associated with the better performance for the 10^{-3} Torr case than for the other two cases. Furthermore, the impedance analysis performed at low overpotential (0.8 V) also displayed an obviously lower polarization resistance of R_p (charge transfer and diffusion resistance) for the 10^{-3} Torr case (0.41 Ω) than for both 10^{-2} and 10^{-4} Torr cases (0.87–0.88 Ω) while their high frequency ohmic resistances (R) were similar (0.43, 0.46, and 0.46 Ω, respectively). The results are consistent with their potential versus current density (performance) curves that the 10^{-3} Torr case had an apparently lower cell potential loss (mainly due to kinetic resistance) in the activation-controlled region than the other two cases. The same is true for the comparison of the 10^{-2} and 10^{-4} Torr cases with the other two 10^{-3} Torr cases (50 and 100 W) chiefly due to higher R_p values for the former cases than the latter cases (0.61–0.63 Ω) whereas the R-values for the four cases were similar at 0.8 V (even at the increased overpotential of 0.7 V) (Fig. 5a and b and Table 2). Neverthe-

less, all the five cases exhibited a slope increase around 0.6 V in the non-kinetically controlled regions of cell polarization curves, suggesting the increasing influence from mass transfer, possibly due to the increasing water accumulation (but not yet the flooding) within the three-phase zone. This phenomenon is also associated with the dense Pt films sputtered on carbon particles in electrode fabrication in this study.

Although the electrode Pt loadings were controlled to be the same for the electrodes prepared at three different pressures, the electrodes made at 10^{-3} Torr exhibited more available sites for hydrogen desorption in CV (Fig. 3) and thus had an evidently greater EAS area than those made at 10^{-2} and 10^{-4} Torr (Table 2), partially responsible for the better electrode/cell performance for the 10^{-3} Torr case than for the 10^{-2} and 10^{-4} Torr cases. The finding implies that the interconnection (contact) of carbon-supported Pt was better for the 10^{-3} Torr case than for the other two cases, and this is possibly associated with the different Pt deposition rates controlled by gas pressure. As stated in Section 3.1, the sputtering system operating at 10^{-3} Torr displayed a higher deposition rate of Pt and needed a shorter sputtering time than those operating at 10^{-2} and 10^{-4} Torr to obtain the same Pt loading. Possibly, the operation using a lower deposition rate and a longer sputtering time enhances the formation of a denser Pt film (or more concentrated configuration of Pt grains) on carbon particles to decrease the EAS area. It is also possible that the operation at the lower sputtering-gas pressure (the 10^{-4} Torr case) had a better collimation to conduct more deposition of Pt in the micropores of carbon particles whereas a higher collision possibility for the Pt atoms bombarded away from a target at the higher sputtering-gas pressure (the 10^{-2} Torr case) might lead to the aggregation of Pt grains to decrease EAS area. The higher EAS area or Pt roughness is also associated with the lower R_p of the 10^{-3} Torr case. Note that the EAS area only accounted for partial activation loss which was also associated with the surface concentrations of the species involved in the electrode reactions, as stated in Section 3.2. The magnitudes of EAS area and reactant concentration on active sites should be related to the microstructure of Pt grains sputtered on carbon particles.

Accordingly, to obtain the best electrode/cell performance at the Pt loading of 0.1 mg cm^{-2}, the optimal RF power and the sputtering-gas pressure were 100 W and 10^{-3} Torr, respectively, in this study. The cathode prepared at the optimal RF power and sputtering-gas pressure exhibited the lowest kinetic resistance. The activation polarization (varying with electrodes) dominated the cell performance because the polarization trends in ohmic-controlled (or concentration-controlled) regions were similar for all the electrodes tested. The results are consistent with that activation overvoltage is the most important irreversibility and cause of voltage drop (mainly occurring at the cathode) in low and medium temperature (hydrogen–oxygen/air) fuel cells [32]. Furthermore, it seems that the control of sputtering-gas pressure is more important than that of RF power in the tested ranges of this work to lower the activation loss. However, the sputter deposition of Pt onto porous carbon particles is complicated, and the electrode microstructure, varying with RF power and sputtering-gas pressure, is crucial to improve the electrode/cell performance.

4. Conclusions

The effects of RF power and sputtering-gas pressure in electrode fabrication on MEA/cell performance were investigated in this study. It was found that the deposition rate of Pt increased with increasing RF power, to reach 0.047, 0.084, and 0.107 mg cm^{-2} min^{-1}, at 50, 100, and 150 W, respectively at 10^{-3} Torr. At 100 W, the deposition rates of Pt were 0.060 and 0.070 mg cm^{-2} min^{-1} for the operations at 10^{-4} and 10^{-2} Torr, respectively.

At a Pt loading of 0.1 mg cm^{-2} and 10^{-3} Torr, the performance of MEAs with the Pt/C cathode prepared at 50 and 150 W were similar but lower than that of the MEA prepared at 100 W, which is mainly attributed to the higher kinetic resistance in oxygen reduction for the former electrodes than for the latter electrode although an opposite trend of their EAS areas was observed for the three electrodes. However, at the same Pt loading operating at the 100 W, in comparison to the electrodes prepared at 10^{-4} and 10^{-2} Torr, the electrode prepared at 10^{-3} Torr exhibited a higher EAS area and a lower kinetic resistance responsible for a better electrode/cell performance. It seems that the control of sputtering-gas pressure is more important than that of RF power in the tested ranges to lower the activation loss. All the electrodes having dense Pt films sputtered on carbon particles exhibited a similar trend in slope increase around 0.6 V in cell polarization curves, possibly due to the increasing water accumulation at active sites.

We believe that the microstructures of the electrodes fabricated at different RF powers and gas pressures are important for the improvement of MEA/cell performance and need to be further studied.

Acknowledgments

The authors would like to thank Professor Wen-Jhy Lee at National Cheng Kung University and Dr. Yi-Yie Yan at Industrial Technology Research Institute for their helps, and the National Science Council of the Republic of China, Taiwan for financially supporting this research under Contract No. NSC-92-2211-E-309-002.

References

[1] R.A. Ristinen, J.J. Kraushaar, Energy and the Environment, Wiley, New York, 1999, p. 293.
[2] A.B. Stambouli, E. Traversa, Renew. Sust. Energ. Rev. 6 (2002) 297.
[3] P. Costamagna, S. Srinivasan, J. Power Sources 102 (2001) 242.

[4] C.K. Witham, W. Chun, T.I. Valdez, S.R. Narayanan, Electrochem. Solid-State Lett. 3 (2000) 497.
[5] W.C. Choi, J.D. Kim, S.I. Woo, J. Power Sources 96 (2001) 411.
[6] V. Mehta, J.S. Cooper, J. Power Sources 114 (2003) 32.
[7] M.S. Wilson, S. Gottesfeld, J. Appl. Electrochem. 22 (1992) 1.
[8] R. O'Hayre, S.-J. Lee, S.-W. Cha, F.B. Prinz, J. Power Sources 109 (2002) 483.
[9] S. Gamburzev, A.J. Appley, J. Power Sources 107 (2002) 5.
[10] G. Bender, T.A. Zawodzinski, A.P. Saab, J. Power Sources 12 (2003) 114.
[11] S. Mukerjee, S. Srinivasan, A.J. Appleby, Electrochim. Acta 38 (1993) 1661.
[12] S.Y. Cha, W.M. Lee, J. Electrochem. Soc. 146 (1999) 4055.
[13] E.J. Taylor, E.B. Anderson, N.R.K. Vilambi, J. Electrochem. Soc. 139 (1992) 45.
[14] M.W. Verbrugge, J. Electrochem. Soc. 141 (1994) 46.
[15] K.H. Choi, H.S. Kim, T.H. Lee, J. Power Sources 75 (1998) 230.
[16] H. Kim, B.N. Popov, Electrochem. Solid-State Lett. 7 (2004) 71.
[17] S. Hirano, J. Kim, S. Srinivasan, Electrochim. Acta 42 (1997) 1587.
[18] E.A. Ticianelli, J.G. Beery, S. Srinivasan, J. Appl. Electrochem. 21 (1991) 597.
[19] W.-T. Li, D.R. McKenzie, W.D. McFall, Q.-C. Zhang, Thin Solid Films 384 (2001) 46.
[20] A. Nagata, H. Okayama, Vacuum 66 (2002) 523.
[21] H.W. Kim, N.H. Kim, Mater. Sci. Eng. B103 (2003) 297.
[22] Z.H. Liu, N.M.D. Brown, Thin Solid Films 349 (1999) 78.
[23] M. Jana, D. Das, Sol. Energ. Mater. Sol. Cells 79 (2003) 519.
[24] T. Biegler, D.A.J. Rand, R. Woods, J. Electroanal. Chem. 29 (1971) 269.
[25] M. Kawamura, T. Mashima, Y. Abe, K. Sasaki, Thin Solid Films 377–378 (2000) 537.
[26] B. Chapman, Glow Discharge Processes: Sputtering and Plasma Etching, Wiley, New York, 1980, pp. 9–13.
[27] V.I. Shulga, Nucl. Instrum. Meth. Phys. Res. B 174 (2001) 423.
[28] C.H. Hsu, C.C. Wan, J. Power Sources 115 (2003) 268.
[29] L. Giorgi, E. Antolini, A. Pozio, E. Passalacqua, Electrochim. Acta 43 (1998) 3675.
[30] E.A. Ticianelli, C.R. Derouin, A. Redonod, S. Srinivasan, J. Electrochem. Soc. 135 (1988) 2209.
[31] A. Damjanovic, V. Brusic, Electrochim. Acta 12 (1967) 615.
[32] J. Larminie, A. Dicks, Fuel Cell Systems Explained, Wiley, England, 2000, p. 45.